Formation of shrinkage porosity during solidification of steel: Numerical simulation and experimental validation

M. Riedler[1], **S. Michelic**[2], **C. Bernhard**[1]
[1] Chair of Ferrous Metallurgy, Montanuniversitaet Leoben, Austria
[2] INTECO TBR casting technologies GmbH, Austria

E-mail: michael.riedler@unileoben.ac.at

Abstract. The phase transformations in solidification of steel are accompanied by shrinkage and sudden changes in the solubility of alloying elements, resulting in negative side effects as micro- and macrosegregation and the formation of gas and shrinkage porosities. This paper deals with the numerical and experimental simulation of the formation of shrinkage porosity during the solidification of steel.
First the physical basics for the mechanism of shrinkage pore formation will be discussed. The main reason for this type of porosity is the restraint of fluid flow in the mushy zone which leads to a pressure drop. The pressure decreases from the dendrite tip to the root. When the pressure falls below a critical value, a pore can form.
The second part of the paper deals with different approaches for the prediction of the formation of shrinkage porosity. The most common one according to these models is the usage of a simple criterion function, like the Niyama criterion. For the computation of the porosity criterion the thermal gradient, cooling rate and solidification rate must be known, easily to determine from numerical simulation. More complex simulation tools like ProCAST include higher sophisticated models, which allow further calculations of the shrinkage cavity.
Finally, the different approaches will be applied to a benchmark laboratory experiment. The presented results deal with an ingot casting experiment under variation of taper. The dominant influence of mould taper on the formation of shrinkage porosities can both be demonstrated by the lab experiment as well as numerical simulations. These results serve for the optimization of all ingot layouts for lab castings at the Chair of Ferrous Metallurgy.

1. Introduction

The solidification process for steel is coupled with volume shrinkage due to an increase in the density with decreasing temperature. This volume shrinkage can be compensated by feeding with liquid steel. As long as feeding is sufficient, porosity will not occur. At the end of solidification the resistance against the flow increases leading to a higher pressure drop and therefore to the formation of shrinkage porosity.

The aim of this paper is to compare experimental investigations regarding shrinkage porosity with numerical result. Therefore ingots with different geometry were cast and cut along the ingot length axis to make the shrinkage porosity apparent. The numerical simulation of the ingots was performed with the software ProCAST. Different porosity criteria and their respective porosity models were used to predict the formation of shrinkage porosity in the ingot. Finally, a comparison between the different numerical and experimental results was made.

2. Theoretical aspects of the formation of porosities

The formation of porosity can be divided into two main categories: gas porosity and shrinkage porosity. The formation mechanism and the porosity shape of both porosity types exhibit substantial differences.

Investigations of gas porosity show that the shape of this porosity type is the most time spherical or sometimes ellipsoid. The formation of gas porosity is based on the fact that the saturation for the important gases [H], [N] and [O] (formation of CO) in liquid steel decreases as the temperature drops, which is depicted in figure 1. The heat withdrawal of the mould lowers the temperature of the liquid steel and leads to an enrichment of gaseous elements at the front or between the dendrite arms. The reason for the formation of gas porosity is due to the gas exceeding its saturation point. The spherical shape of this porosity type implies that the formation occurs in the liquid state or during the early stage of solidification. At the end, it is of note that the nucleation of gas porosity is not homogeneous as the internal pore pressure would be very high. Therefore, heterogeneous nucleation is preferable, and, hence, inclusions or uneven surfaces will be used as a nucleation site. [1], [2], [3]

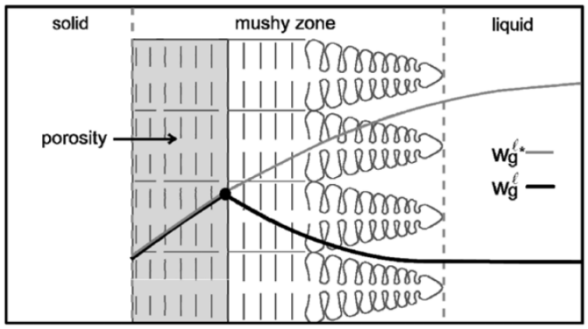

Figure 1. Schematic illustration of the raising gas concentration w^l_g in the mushy region based on gas microsegregation and the diminution of the solubility limit $w^{l*}_g(T,p_l)$ [2], [3].

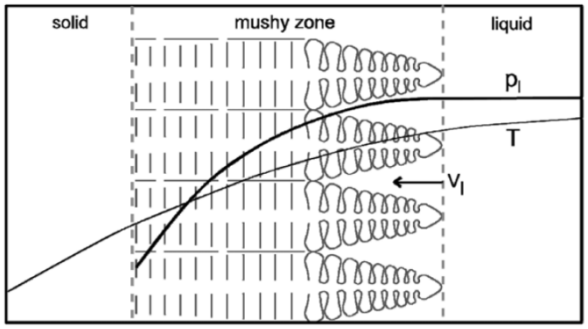

Figure 2. Schematic illustration of the liquid pressure drop in the mushy region based on solidification shrinkage[2], [3].

In contrast to gas porosity the shape of shrinkage porosity is very tortuous and is dendritic solidifying alloys limited by the primary dendrites and dendrite arms. Shrinkage porosity appears at the end of solidification range and so the shape of this type is adjusted by the remaining space between the dendrites. The shrinkage effect of the steel due to decreasing temperature can be compensated in the mushy zone by feeding liquid steel. This can be a problem for wide range mushy zones as the fluid flow of the liquid steel must be sufficient down to the root of the dendrite. The restraint of the fluid flow in the mushy zone leads to a pressure drop, as illustrated in figure 2. An inadequate development of the interdendritic flow reduces the pressure to a certain limit, which leads to an insufficient feeding, and, to the formation of shrinkage porosities. Thus, it is clear that the formation of this porosity type occurs at the end of the solidification range and furthermore, the shape is related to the remaining space of the dendrites. Finally, a 2D metallographic image shows only a small part of this porosity type (size is around a few tens of micrometers), as it normally interconnects in a complex manner and only a 3D illustration can capture the full extension. [1], [2], [3]

3. Prediction of the formation of shrinkage porosity

Thus far, many methods for the prediction of the appearance of shrinkage porosity exist. These methods range from very simple methods, which use only material properties or solidification parameters, to highly complex methods, which are the mostly self-programmed and try to explain the formation. To calculate the shrinkage porosity for an ingot, the Niyama criterion and the porosity algorithm of ProCAST are used in this work. These methods are explained in detail below.

3.1. Porosity Criterion

Niyama et al. [4] established a criterion to determine the appearance of shrinkage porosities. Therefore they considered different porosity criterion which can be calculated easily and compared these values with experimental results. As a result a porosity criterion was investigated, which is now widely used and known as Niyama criterion. The criterion can be calculated with the following equation (1)

$$Ny = \frac{G}{\sqrt{\dot{T}}} < 1 \tag{1}$$

where G is the thermal gradient and $\dot{T}$ is the cooling rate. Regarding steel, the critical value is around 1.0 [(K min)$^{0.5}$/cm]. A Niyama value below this critical value leads to the occurrence of shrinkage porosity. The advantage of this criterion is the independence of the casting geometry. Nevertheless, the critical value depends on the corresponding casting material and must be determined for every casting material. [5], [6], [7], [8]

The Niyama criterion was further developed by Carlson et al. [9]. The aim of this improvement was to predict not only the position of the shrinkage porosity in the casting, but also the amount of the pore volume fraction. The advanced Niyama criterion is also called the dimensionless Niyama criterion and can be calculated according to equation (2)

$$Ny^* = \frac{G\,\lambda_2\sqrt{\Delta P_{cr}}}{\sqrt{\mu_l \beta \Delta T_f \dot{T}}} = Ny\frac{\lambda_2\sqrt{\Delta P_{cr}}}{\sqrt{\mu_l \beta \Delta T_f}} = \sqrt{I(g_{l,cr})} \tag{2}$$

where λ_2 is the secondary dendrite arm space, ΔP_{cr} is the critical pressure drop; μ_l is the liquid dynamic viscosity; $\beta = (\rho_s - \rho_l)/\rho_l$ is the solidification shrinkage; $\Delta T_f = T_{liq} - T_{sol}$ is the freezing range and $I(g_{l,cr})$ is an integral, which depends on the solid fraction-temperature curve. For simple curves the integral can be calculated analytically with equation (3)

$$I(g_{l,cr}) = \int_{g_{l,cr}}^{1} 180\,\frac{(1-g_l)^2}{{g_l}^2}\frac{d\theta}{dg_l}\,dg_l \tag{3}$$

where $\theta = (T - T_{sol})/\Delta T_f$ is the dimensionless temperature. Further details regarding the dimensionless Niyama criterion can be found in [9]. Carlson et al. uses the dimensionless Niyama criterion to understand the formation of shrinkage porosity for an aluminium alloy, a magnesium alloy and mild steel. Further verification using casting experiment with steel was made

3.2. Porosity model of ProCAST

ESI Group has implemented a model to predicting shrinkage porosity into the software ProCAST. Two important parameters are needed to calculate the porosity. The first parameter is MacroFs which corresponds to a solid fraction and defines the starting point for the porosity calculation. The second parameter is called FeedLen and can be seen as an interdendritic feed length. The porosity calculation is performed for regions with a solid fraction between MacroFs and 1. For these areas two possible situations can occur:

1. The mushy zone contains regions with a solid fraction lower than MacroFs

   In this case the distance between the solidus temperature isotherm and the MacroFs isotherm is calculated. The distance between these isotherms must be larger than FeedLen for the formation of porosity. Hence, a high temperature gradient leads to a smaller distance and vice versa, which is schematically illustrated in figure 3. The temperature gradient in region A is low and therefore the distance between the two isotherms is greater than FeedLen. Porosity will form in this area. In zone B, the distance is smaller since the gradient is much higher and as a consequence no porosity will occur. [10]

2. All elements in the mushy zone have a solid fraction higher or equal than MacroFs

The appearing shrinkage between MacroFs and solidus temperature is compensated through the formation of porosity in the whole region. [10]

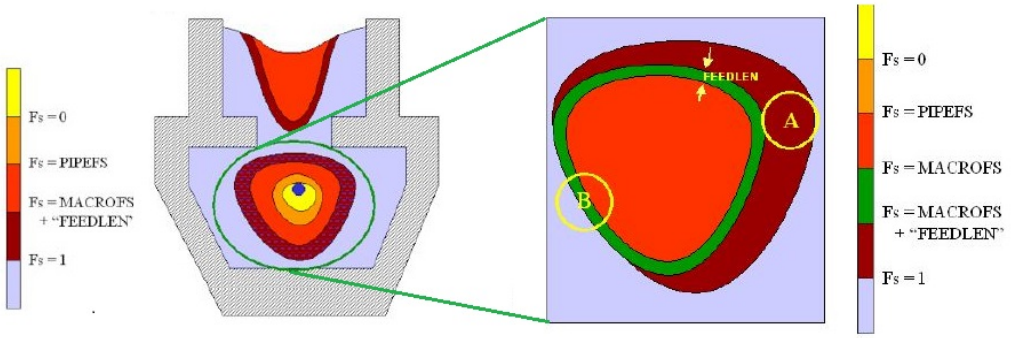

Figure 3. Schematic illustration of the internal shrinkage porosity calculation from ProCAST [10].

4. Development of the experimental casting trials

Casting trials were performed in the melt shop of the Chair of Ferrous Metallurgy in Leoben. Thereby the geometries of the mould were varied to see whether there is an influence on porosity formation.

At the top of the ingot a feeding head is installed to influence the solidification behaviour in this region. Furthermore, please note that the mould is not completely filled with liquid steel. The meniscus level of the liquid steel is around 30 mm beneath the top edge of the mould. Thus the ingot has dimensions of 100 mm x 100 mm x 370 mm and a weight around 27 kg. The inner surface of the mould was covered with release agents for a better separation. For a better stability the mould was embedded into sand. Three experimental trials were cast with varying taper which changed from 0° to 5° and 10° only for the narrow mould wall. The broader mould side is parallel. Furthermore, the mould was not heated up before casting. At the end of casting experiment the top of the ingot were covered with an insulation powder. The steel was cast into the mould by use of the top pouring method.

From the literature it can be seen that the formation of shrinkage porosity depends on the material. A material with a wide-spread mushy zone tends to form porosities as a material with a narrow mushy zone. Thus, steel with a high carbon content was used as cast material. The composition of the cast steel is shown in table 1. For the mould a common structural steel (S 335) was used.

Table 1. Steel composition of the ingot

	C [wt.-%]	Si [wt.-%]	Mn [wt.-%]	Al [wt.-%]
Cast Material	0.85	0.30	1.00	0.04

An important part of the metallographic examinations is the detection of shrinkage porosity. For this purpose, a 10 mm slice was cut out at the middle of the ingot. A macroscopic image was made to identify the porosity in the ingot centre.

5. Modelling of the experiment

The simulation of the solidification process was performed with the finite element software ProCAST from ESI Group. The software has the ability to solve the transient behaviour of a three dimensional thermal and fluid flow problem. ESI Group introduced a new discretization method called edge-based finite element method (EBFEM) in the version 2013.0. EBFEM uses an up-winding scheme with limiters to discretize the advection operator, thereby leading to a higher-order of accuracy and rendering an improved mould filling behaviour. Furthermore, ESI Group have implemented an

adapted solver into ProCAST 2013.0. The solver based on the algebraic multigrid method and is a robust and highly powerful linear solver. [10], [11], [12]
ProCAST solves following partial differential equations:

- Momentum balance for the velocities U, V and W
- Mass balance for the pressure P
- Energy balance

5.1. General simulation scheme

The ingot dimensions necessitate a 3D simulation as the third dimension has an influence on the results. There were several constraints regarding the setup of the model:

- mould filling process is not calculated
- formation of the pipe is not considered
- only natural convection is simulated

For the discretization of the geometry, a structured mesh grid was used. The average size of the element was 5 mm, which leads to a total number of elements of around 85000. A simple permeability model, which is widely used, was applied at these simulations. The Carmen-Kozeny model is an isotropic permeability model and based on the pressure drop during the flow of a fluid through a porous medium. Equation (4) describes this model.

$$K = K_0 \frac{{g_l}^3}{(1-g_l)^2} \tag{4}$$

K_0 represents the microstructure of the steel and can be calculated with $K_0 = {\lambda_2}^2/180$; λ_2 is the secondary dendrite arm space. For the calculation of the permeability a secondary dendrite arm space λ_2 of 50 µm was estimated.

5.2. Material properties

ProCAST can handle temperature-dependent material data which are used for these simulations. The material data are calculated for cast and mould material with the software IDS [13]. The software was developed from Miettinen et al. to determine the material data for low alloyed steel and consider further a microsegregation model. The insulation at the top of the ingot is a typical ceramic material, thus typical properties for such a material are used. [14], [15]

5.3. Initial and boundary condition

For the simulation a superheat of 15 °C was used. The initial temperature of the mould was assumed to have an elevated room temperature of 40 °C. The majority of the ingot's heat and also mould will be removed through heat conductivity as the mould is embedded into sand. Hence, the applied boundary conditions for the mould surface is a heat transfer coefficient of 200 [W/(m²K)] at an ambient temperature of 25 °C. It is assumed that no heat radiation between mould and sand occurs. Therefore the emissivity was set to 0. The top of ingot is covered with an insulation powder. For the sake of simplicity, this powder was not explicitly defined at the model. However, the influence of the powder is considered since an adiabatic boundary condition was used. The interface heat transfer coefficient between ingot and mould should be determined with temperature measurement and an inversion calculation. Unfortunately the measurements were not successfully or recorded unrealistic temperatures. Therefore an assumption must be made for these values. The interface heat transfer coefficient between mould and ingot was assumed to be 150 [W/(m²K)] and between insulation and mould respectively ingot a value of 100 [W/(m²K)] was set.

5.4. Possibilities to calculate the porosity formation

ProCAST offers many possibilities to calculate porosity criteria, especially the Niyama criterion. It is possible to compute this criterion during the simulation or afterwards in the post processing menu. In

this case the Niyama criterion was calculated during the simulation and a solid fraction of 0.9 was used. To calculate the dimensionless criterion, a critical pressure drop ΔP_{cr}, and also the secondary dendrite arm space λ_2 must be defined. In this case ΔP_{cr} is assumed at 1.01 bar, which corresponds to a liquid pressure of 1.01 bar and no capillary pressure; λ_2 is set to 200 µm which should be a good assumption for the ingot centre. The other parameter can be calculated from the material properties. Furthermore, it is possible to use the internal model from ProCAST. Therefore the parameter MacroFs and FeedLen must be defined. For theses simulations the parameter MacroFs is set to 0.85 and FeedLen is 5 mm. [10]

6. Results

The primary structure of the cast ingots with a mould taper of 0°, 5° and 10° are depicted at figure 4. The shrinkage porosity is marked with a green colour in this picture.

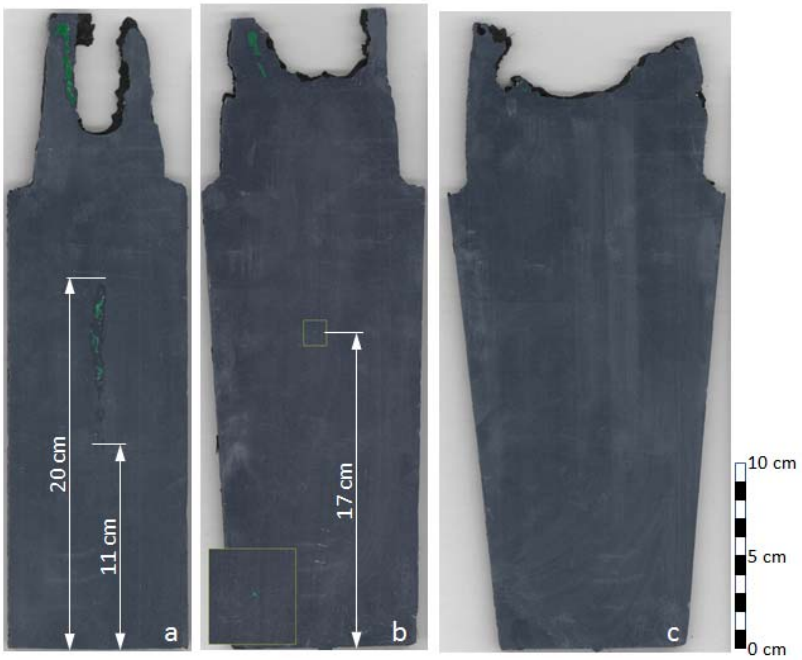

Figure 4. Experimental results of the cast ingots (a: 0° taper; b: 5° taper; c: 10° taper).

On the left, the ingot with no taper is shown. As can be seen from the image, shrinkage porosity appears at the centre of the ingot and extends from 11 cm to 20 cm ingot height. For an ingot with a 5° taper, a small pinhole at 17 cm is detectable. The ingot with a 10° taper is free of shrinkage porosity. Furthermore, it is clear to see how the pipe geometry changes with the mould taper. Looking at the ingot with no taper, the pipe is very deep. However, this changes with a higher mould taper to a flatter and wider pipe.

The Niyama criterion for the ingot with no taper is illustrated in figure 5. As mentioned above, shrinkage porosity will appear if the Niyama criterion falls below 1 $[(K\ min)^{0.5}/cm]$. The criteria have low values at the centre of the ingot an also in the top. A 2D plot of the ingot centre axis is shown in figure 6 for different mould tapers. The difference between the behaviour of the Niyama value seems to be minor, but it is clear to see that the minimum Niyama value for an ingot with no taper falls below 1 $[(K\ min)^{0.5}/cm]$ and for an ingot with 10° taper it exceeds 1 $[(K\ min)^{0.5}/cm]$. The simulation describes the experimental results very well. The position of the minimum Niyama values matches quite well with the experimental results.

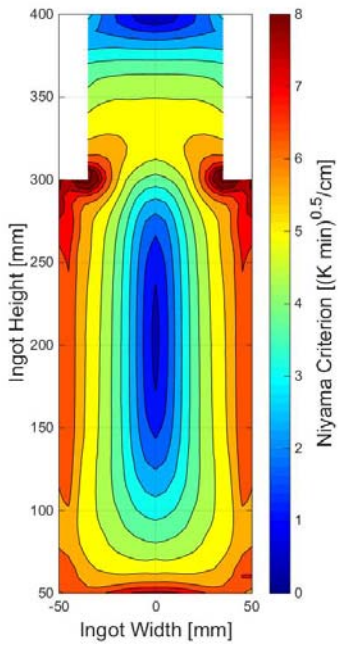

Figure 5. Calculated Niyama criterion for cast ingot with no taper.

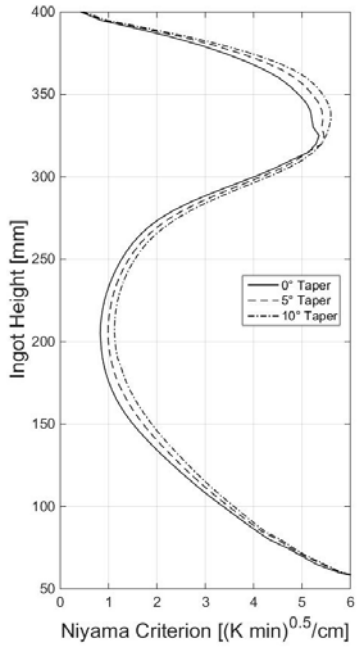

Figure 6. Comparison of the Niyama criterion for three ingots with different taper.

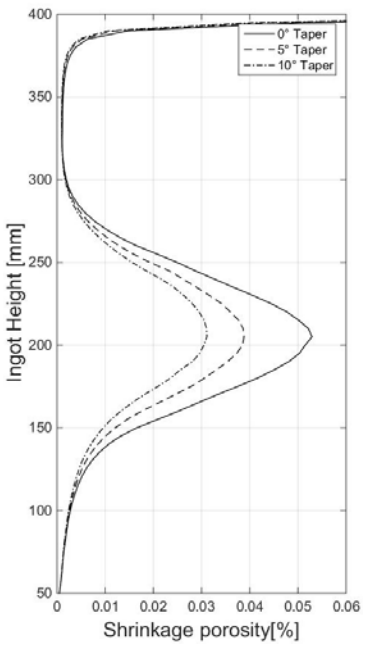

Figure 7. Comparison of the shrinkage porosity for three ingots with different taper.

Using the dimensionless Niyama criterion it is possible to predict the shrinkage porosity amount for the cast ingots. The linkage between the Niyama value and the shrinkage porosity percentage is depicted in figure 8. The calculated distribution of the pores is centred on the middle of the ingot and decreases rapidly outside the centre.

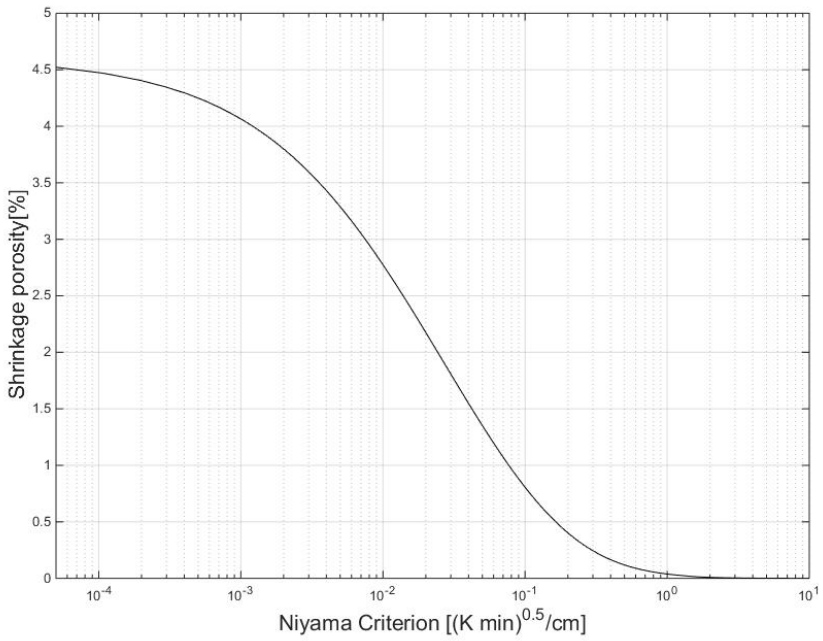

Figure 8. Relation between Niyama criterion and shrinkage porosity.

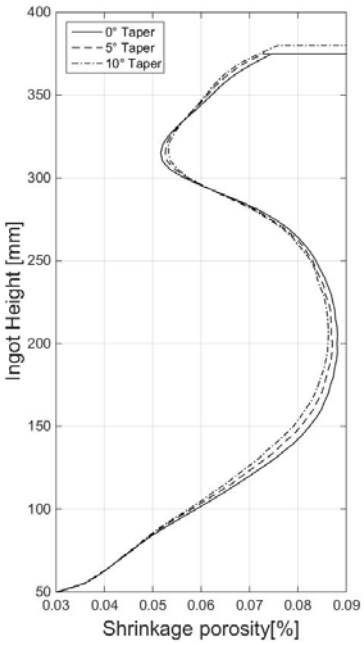

Figure 9. Comparison of porosity amount using the ProCAST internal method

Figure 7 shows the amount of shrinkage porosity in the ingot centre for different mould taper. It is obvious that the amount decreases with increasing taper. The amount of shrinkage porosity calculated with ProCAST internal model is depicted in figure 9. The position of maximum shrinkage porosity is the same for both calculation methods. Comparing the amount of the occurring porosity the method after Carlson et al. is about 40 % lower than with the use of the ProCAST internal method. The amount and also distribution of the pores calculated with the ProCAST internal model is higher and more uniform than the dimensionless Niyama criterion. Hence, the distinction of the shrinkage porosity between different taper dimensions is tiny when using the internal method.

7. Conclusion

Experimental investigations were made regarding the correlation between mould taper and shrinkage porosity. For this purpose, three ingots with different tapers (0°, 5°and 10°) were cast. The amount of the centre porosity decreases with increasing mould taper, which reflects the literature. The ingot with a 10° taper has no visible porosity. Further efforts were made to model the cast ingots and implement the Niyama criterion to obtain information about porosity formation. The Niyama criterion for the ingot with a 10° taper does not fall below a critical value of 1 [$(K\ min)^{0.5}$/cm], and, consequently no porosity appears. This is in good agreement with the experimental results. The Niyama value for the ingot with no taper is below 1. Therefore, shrinkage porosity will occur. The position of this formation regarding the ingot height is slightly higher compared to the experimental results.

Using the dimensionless Niyama criterion it is not only possible to predict the formation of shrinkage porosity, but also the amount of porosity can also be determined. It can be seen that the amount of shrinkage porosity decreases from 0.05% to 0.03% with increasing mould taper. ProCAST has also the ability to calculate the amount of shrinkage porosity. The calculated porosity percentage (by use of the ProCAST internal method) is approximately two-thirds higher when compared to the dimensionless Niyama criterion. Moreover, the distribution of the shrinkage porosity is more uniform.

8. References

[1] Dantzig J A and Rappaz M 2009 Solidification (Lausanne: EPLF Press)
[2] Couturier G and Rappaz M 2006 *Model. Simul. Mater. Sc.* 253–71
[3] Couturier G and Rappaz M 2006 Modeling of porosity formation in multicomponent alloys in the presence of several dissolved gases and volatile solute elements *Symp. on Simulation of Aluminum Shape Casting Processing (San Antonio, Texas, USA)* pp 143-52
[4] Niyama E, Uchida T, Morikawa M and Saito S 1982 *AFS Int. Cast Met. J.* **7** 52–63
[5] Stefanescu D M 2005 *Int. J. Cast Metal. Res.* **18** 129–43
[6] Stefanescu D M 2009 Science and Engineering of Casting Solidification (New York, NY: Springer Science + Business Media)
[7] Carlson K D, Ou S, Hardin R A and Beckermann C 2002 *Metall. Mater. Trans. A* **33** 731–40
[8] Sigworth G K and Wang C 1993 *Metall. Mater. Trans. B* **24** 349–64
[9] Carlson K D and Beckermann C 2009 *Metall. Mater. Trans. A* **40** 163–75
[10] ESI Group 2013 ProCAST 2013.5: *User's Manual* (Paris: ESI Group)
[11] Sang B, Kang X and Li D 2010 *J. Mater. Process. Tech.* **210** 703–11
[12] Orgeas L, Gabathuler J P, Imwinkelried T, Paradies C and Rappaz M 2003 *Model. Simul. Mater. Sc.* **11** 553–74
[13] Miettinen J, Lauhenkiipi S and Laine J 1997 IDS - Solidification Analysis Package (Helsinki: Helsinki University of Technology)
[14] Miettinen J 1997 *Metall. Mater. Trans. B* **28** 281–97
[15] Miettinen J, Louhenkilpi S, Kytönen H and Laine J 2010 *Math. Comput. Simulat.* **80** 1536–50